Characterization of hot deformation behaviour of Nb-Ti microalloyed high-strength steel

G-L. Wu[1], Y-J. Zhang[1], and S-W. Wu[1]

Affiliation:
[1]School of Minerals Processing and Bioengineering, Central South University, China.

Correspondence to:
Y-J. Zhang

Email:
zhangyongji_csu@163.com

Dates:
Received: 23 Aug. 2017
Revised: 20 Oct. 2018
Accepted: 14 Nov. 2018
Published: May 2019

How to cite:
Zhang, Y-J.
Characterization of hot deformation behaviour of Nb-Ti microalloyed high-strength steel.
The Southern African Insitute of Mining and Metallurgy

DOI ID:
http://dx.doi.org/10.17159/2411-9717/17/380/2019

ORCiD ID:
Y-J. Zhang
https://orchid.org/0000-0002-8216-2091

Synopsis

The hot deformation behaviour of Nb-Ti microalloyed high-strength steel was investigated. Hot compression tests were conducted in the temperature range 900 to 1100°C under strain rates of 0.1, 1, and 5 s^{-1}. Dynamic recrystallization (DRX) occurs as the main flow softening mechanism at high temperature and low strain rate. The hot deformation activation energy was calculated to be about 404 699 J/mol. The constitutive equation was developed to describe the relationship between peak stress, strain rate, and deformation temperature. The characteristics of DRX at different deformation conditions were extracted from the stress-strain curves using the work hardening parameter. The Cingara-McQueen equation was developed to predict the flow curves up to the peak strain. The processing maps were obtained on the basis of a dynamic materials model. The results predict an instability region in the temperature range 1010 to 1100°C when the strain rate exceeds 0.78 s^{-1}.

Keywords
flow stress; high-strength steel; constitutive model; material constants; processing map.

Introduction

The 700 MPa grade HSLA steel is widely used in engineering machinery, automotive beams, carriages, and axle tubes, *etc.* (Pan *et al.*, 2017). Generally, such grades contain a moderately high amount of Mn (approx. 1.4% and above), and microalloying elements like Nb, Ti, V, and Mo to impart the desired strength and toughness through solid-solution strengthening, precipitation hardening, and grain refinement dislocation strengthening (Chen and Yu, 2012; Opiela, 2014). However, the production costs can be greatly reduced by replacing part of the Nb, V, or Mo with inexpensive Ti and adopting the compact strip production CSP process (Opiela, 2014; Chen *et al.*, 2015). Furthermore, the microalloying technology coupled with new-generation thermomechanical control processing (NG-TMCP) has proved efficient for achieving the proper balance between strength, toughness, ductility, and formability by means of a suitable combination of chemical composition and thermomechanical treatment parameters (Shukla *et al.*, 2012; Wu, Zhou, and Liu, 2017).

In hot forming processes, the complex microstructural evolutions are often induced by multiplicative hot deformation mechanisms, such as work hardening (WH), dynamic recovery (DRV), and dynamic recrystallization (DRX) (Zhang *et al.*, 2014; Liang *et al.*, 2015). Dynamic softening behaviour during hot processing has generated considerable interest because component properties are influenced significantly by its corresponding microstructural evolution (Wu *et al.*, 2010). During deformation in the DRX process, deformed grains are replaced with substructures and newly formed fine and uniformly distributed grains. This occurs only when a critical strain for the onset of DRX is reached, and at the same time, the minimum rate of energy dissipating is reached (Ferdowsi *et al.*, 2014). DRV occurs at a high strain rate and low temperature, reducing the stored energy greatly and making DRX difficult (Liang *et al.*, 2015). The microstructural changes during DRX are sensitive to the processing parameters, such as strain rate, deformation temperature, and strain (Zhang *et al.*, 2014; Ferdowsi *et al.*, 2014). Therefore, in order to optimize the hot processing parameters, it is important to understand the behaviour of hot deformation *vis-à-vis* control of microstructural evolution.

Constitutive equations are widely used to reveal the relationship between stress and strain at different strain rates or temperatures, providing microstructural information related to the mechanisms of hot deformation. The modelling of the hot flow stress and the prediction of flow curves are employed in rolling and forging processes from the mechanical and metallurgical standpoints (Cabrera *et al.*, 1997; Mirzadeh, Cabrera, and Najafizadeh, 2012). Since DRX is an important metallurgical phenomenon for controlling

microstructural evolution during hot working, the prediction of the critical stress for initiation of DRX is of significant importance in modeling hot working processes. However, the concomitant occurrence of different metallurgical mechanisms during hot working makes it difficult to exactly predict the critical stress for onset of DRX from the true stress–true strain curve. Earlier studies (Poliak and Jonas, 2003; Mirzadeh and Najafizadeh, 2010) showed that the critical conditions for DRX initiation can be obtained by using the relationship between WH rate and stress. Hence predicting peak stress characteristics during hot deformation using appropriate constitutive models is essential in order to understand the microstructural evolution mechanisms.

The dynamic materials model (DMM) was developed for studying the workability parameter, based on principles of continuum mechanics of large plastic flow using the concepts of physical systems modelling and extremum principles of irreversible thermodynamics (Banerjee, Robi, and Srinivasan, 2012). A processing map based on the DMM and consisting of the efficiency map and the instability map is a valuable approach for coupling the processing conditions such as deformation rate and temperature with desired microstructure to optimize the deformation process (Lou *et al.*, 2014). For optimizing hot workability and controlling the microstructure, DRX is a chosen domain. On the one hand, the damage processes are sometimes very efficient in dissipating power for the generation of new surfaces. On the other hand, the safe processes may become less efficient, because power dissipates through the annihilation of dislocations (Banerjee, Robi, and Srinivasan, 2012). In recent investigations, the constitutive equation and processing map have been proposed for steel (Churyumov *et al.*, 2015; Guo *et al.*, 2012), Al-based alloys (Li *et al.*, 2015), Ni-based alloys (Chen *et al.*, 2015), Ti-based alloys (Quan *et al.*, 2015), composite materials (Momeni, Dehghanib, and Poletti, 2013; Rajamuthamilselvan and Ramanathans, 2012) and other materials (Wang *et al.*, 2015).

In order to control the production cost of 700 MPa grade HSLA steel, the composition design and process optimization were investigated. The Mn and Nb contents of the steel were reduced without adding Mo, while the Ti content was increased. A comprehensive understanding of hot deformation characteristics can elucidate the best design of a processing route such as hot rolling or thermomechanical processing. Therefore, the hot deformation behaviour of Nb-Ti HSLA steel was studied in this work. The experimental results have a certain practical significance for the high-temperature deformation of Nb-Ti HSLA steel.

Experimental

The chemical composition of the investigated steel is shown in Table I. Cylindrical hot compression specimens 12 in mm height and 8 mm in diameter of were machined. In order to minimize the friction between the specimens and die during hot deformation, the flat ends of the specimen were recessed to a depth of 0.1 mm to entrap the lubricant of graphite mixed with machine oil.

Table I

Chemical composition of the experiment material (mass %)

C	Si	Mn	P	S	Al	Nb	Ti
0.04	0.01	0.78	0.015	0.007	0.023	0.048	0.11

The hot compression tests were performed on a Gleeble 3500 thermomechanical simulation machine in the temperature range 900 to 1100°C at 50°C intervals under constant strain rates of 0.1, 1, and 5 s^{-1} up to a true strain of 0.7. Each specimen was heated to 1200°C at a rate of 10°Cs^{-1} and held for 180 seconds, and then cooled to the deformed temperature at a cooling rate of 5°Cs^{-1} and held for 30 seconds before deformation for temperature equalization. After deformation, the specimens were immediately quenched in tap water. Throughout each test, high-purity argon was used as protective gas.

Results and discussion

Flow curves analysis

The typical true stress–true strain curves of the steel obtained at various deformation temperatures and strain rates are presented in Figure 1. Based on these curves, the flow stress is sensitive to the deformation temperature and strain rate. In the initial stages of deformation, the flow stress increases rapidly until a peak stress, which indicates that work hardening plays a dominant role. After the rapid flow stress increase, the flow stress decreases slowly as the deformation proceeds until a relatively stable stress appears, indicating a dynamic flow softening. DRX begins to play a dominant role when the strain exceeds peak strain. As the strain increases continually, it enters a steady-state region. Finally, the curves show the equilibrium between work hardening and work softening

Before the stress reaches the peak stress, the work hardening and dislocation density increase, which will lead to a critical microstructural condition. Therefore, the flow stress increases up to a maximum value but the rate of increase steadily decreases until the softening mechanism prevails over work hardening (Solhjoo, 2010). The typical form of the DRX flow curve is observed at high temperatures and low strain rates. At high strain rates, deformation decelerates the rate of work softening (Momeni *et al.*, 2012). Other researchers (Ferdowsi *et al.*, 2014; Mirzadeh, Cabrera, and Najafizadeh, 2012) also point out that higher temperatures and lower strain rates promote the softening process by increasing the mobility of grain boundaries and providing a longer time for dislocation annihilation and the occurrence of DRX.

Establishment of constitutive equations

Hot working can be considered as a thermally activated process, and it can be described by strain rate equations. The relationship between flow stress, strain rate, and temperature can be

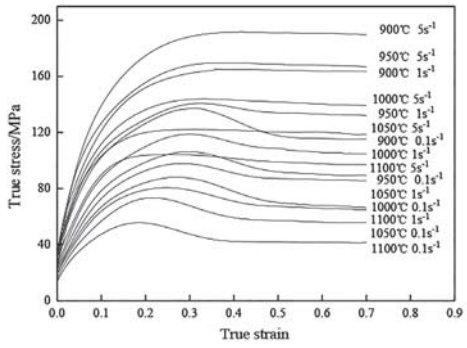

Figure 1—Stress-strain curves of Nb-Ti microalloyed high-strength steel at different deformation temperatures and strain rates

expressed by the hyperbolic sine law (Equation [1]), exponential law (Equation [2]), and power law (Equation [3]) (Ferdowsi *et al.*, 2014, Mirzadeh, Cabrera, and Najafizadeh, 2012):

$$\dot{\varepsilon} = A[\sinh(\alpha\sigma_p)]^n \exp(-\frac{Q}{RT}) \quad [1]$$

$$\dot{\varepsilon} = A_2 \exp(\beta\sigma_p) \quad [2]$$

$$\dot{\varepsilon} = A_1\sigma_p^{n_1} \quad [3]$$

where $\dot{\varepsilon}$ is the strain rate (s^{-1}), σ_p is the peak stress (MPa), and Q is the activation energy for deformation (J/mol). A, A_1 A_2, β, α, n, and n_1 are material constants, and R is the universal gas constant (8.314 J/mol/K).

Taking natural logarithms of both sides of Equations [2] and [3] at a constant temperature yields:

$$\sigma_p = \frac{1}{\beta}\ln\dot{\varepsilon} - \frac{1}{\beta}\ln A_2 \quad [4]$$

$$\ln\sigma_p = \frac{1}{n_1}\ln\dot{\varepsilon} - \frac{1}{n_1}\ln A_1 \quad [5]$$

Substituting the values of the flow stress and corresponding strain rate into Equations [4] and [5] gives the relationship between the flow stress and strain rate, as shown in Figure 2. The values of β and n_1 obtained are 0.073 and 8.31 respectively. The value of the constant α is derived by the division of β by n_1 (Ferdowsi *et al.*,2014; Mirzadeh, Cabrera, and Najafizadeh, 2012), which yields 0.0087.

Taking natural logarithms of both sides of Equation [1] and rearranging, the following equation is derived:

$$\ln[\sinh(\alpha\sigma_p)] = \frac{\ln\dot{\varepsilon}}{n} + \frac{Q}{nRT} - \frac{\ln A}{n} \quad [6]$$

Partially differentiating Equation [6] at constant temperature and strain rate respectively yields:

$$n = \frac{\partial\ln\dot{\varepsilon}}{\partial\ln[\sinh(\alpha\sigma_p)]} \quad [7]$$

$$Q = Rn\frac{\partial\ln[\sinh(\alpha\sigma_p)]}{\partial\frac{1}{T}} \quad [8]$$

The value of n can be derived from the average slope of the lines in $\ln[\sinh(\alpha\sigma_p)]$ *versus* $\ln\dot{\varepsilon}$, shown in Figure 3a. The value of n is calculated to be 6.2. Similarly, the value of Q is determined from the slope of $\ln[\sinh(\alpha\sigma_p)]$ *versus* $1/T$ through averaging the slope values at different strain rates shown in Figure 3b; the Q value is obtained as 404 699 J/mol. The value of lnA can be derived by substituting the obtained values into Equation 6. Thus lnA is calculated to be 37.03.

Substituting all the obtained values into Equation [1], the constitutive equation can be expressed as

$$\dot{\varepsilon} = 1.20\times10^{16}\times [\sinh(0.0087\sigma_p)]^{6.20}\exp(-\frac{404699}{RT}) \quad [9]$$

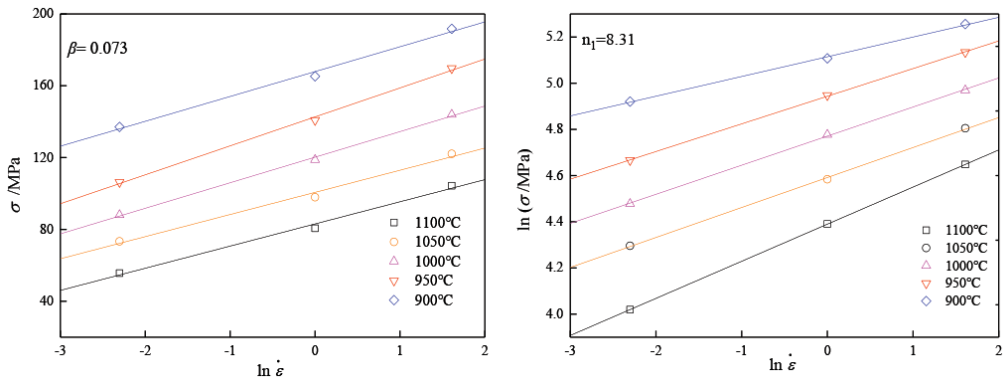

Figure 2—The relationship between flow stress and strain rate according to (a) the exponential law and (b) the power law

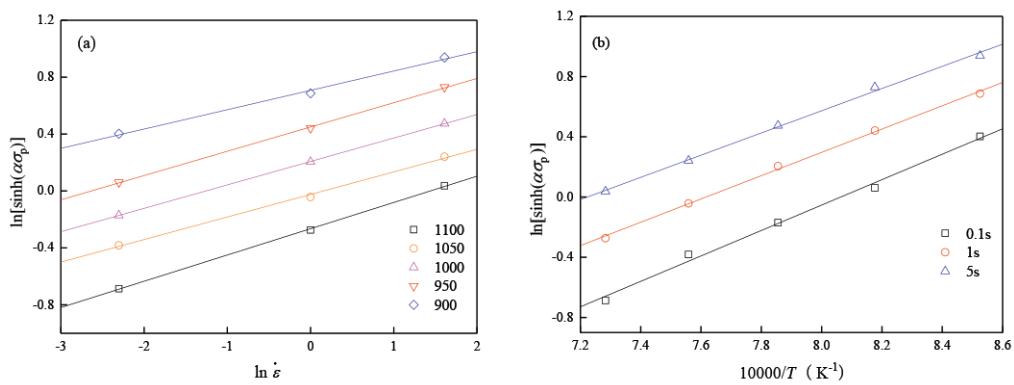

Figure 3—Linear relationship between (a) $\ln[\sinh(\alpha\sigma_p)]$ and $\ln\dot{\varepsilon}$, (b) $\ln[\sinh(\alpha\sigma_p)]$ and $1/T$ for Nb-Ti microalloyed high-strength steel

Equation [9] describes the quantitative relationship between peak stress and the parameters, which reflects the influence of deformation temperature and strain rate on the hot deformation flow stress.

Determination and modelling of critical strain

Generally speaking, DRX can be initiated at a critical level of stress accumulation during hot deformation. However, DRX actually starts at a critical strain (ε_c) which is lower than the strain at peak stress. Only when the strain exceeds ε_c does DRX occur during hot deformation. Therefore it is important to accurately confirm the value of ε_c in the research of hot deformation parameters.

On the flow curve, the point at which the strain hardening rate equals zero represents the peak stress (σ_p) and the inflection point indicates the critical stress (σ_c) for the initiation of DRX. The critical strains can be determined from the inflection points of the $\ln\theta$-ε plots, and the critical stresses can be subsequently obtained either from the θ-σ plots or from the initial flow curves (Poliak and Jonas, 2003).

$$\ln\theta = A_1\varepsilon^3 + A_2\varepsilon^2 + A_3\varepsilon + A_4 \quad [10]$$

where A_1, A_2, A_3, and A_4 are constant parameters for each deformation condition. The second derivative of Equation [10] with respect to ε can be expressed as:

$$\frac{d^2\ln\theta}{d\varepsilon^2} = 6A_1\varepsilon + 2A_2 \quad [11]$$

At the critical stress for initiation of DRX, the second derivative becomes zero. Therefore

$$\varepsilon_c = -A_2/(3A_1) \quad [12]$$

The peak and critical stresses and strains for temperatures of 900, 950, 1000, 1050, and 1100°C at strain rates of 0.1, 1, and 5 s^{-1} are summarized in Table II, and the data is linear fitted as shown in Figure 4. The normalized critical strain ($\varepsilon_c/\varepsilon_p$) can be presented as:

$$\varepsilon_c/\varepsilon_p = 0.41 \quad [13]$$

The relationship between characteristics of DRX and hot deformation parameters

The critical strain varies with strain rate and deformation temperature. The relationship can be described by the Sellars model (Yang *et al.*, 2014):

$$\varepsilon = AZ^n \quad [14]$$

where A and n are material constants, Z is the Zener-Hollomon parameter, and Q is the deformation activation energy (J/mol). Taking the natural logarithm on both sides of Equation [14]:

$$\ln\varepsilon = \ln A + n\ln Z \quad [16]$$

The relationship between $\ln\varepsilon$ and $\ln Z$ is depicted in Figure 5.

Figure 5 exhibits the linear regression results of critical and peak strain versus the Zener-Hollomon parameter. It can be seen that the critical characteristics of DRX increase with increasing Z parameter. The relationship between these parameters and deformation conditions is expressed by a power law. According to the linear regression results, the following relationships hold for the investigated steel:

$$\varepsilon_c = 0.0064Z^{0.077} \quad [17]$$

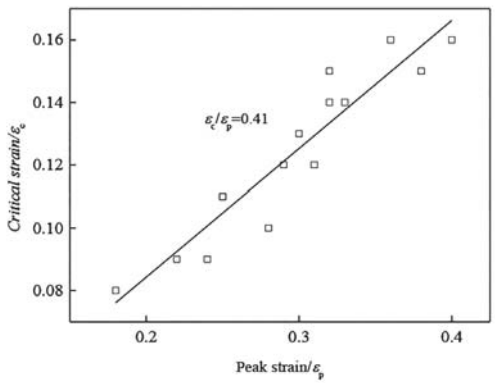

Figure 4—Critical strain *versus* peak strain

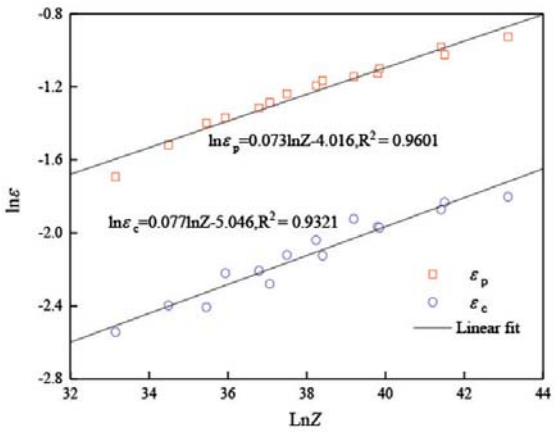

Figure 5—The relationship between ε_c, ε_p, and the *Z* parameter

Table II

Critical strain and peak strain at different deformation conditions

Temperature (°C)	0.1 s^{-1}			1 s^{-1}			5 s^{-1}		
	ε_c	ε_p	$\varepsilon_c/\varepsilon_p$	ε_c	ε_p	$\varepsilon_c/\varepsilon_p$	ε_c	ε_p	$\varepsilon_c/\varepsilon_p$
900	0.15	0.32	0.45	0.16	0.36	0.44	0.16	0.40	0.42
950	0.12	0.29	0.41	0.14	0.32	0.43	0.15	0.38	0.41
1000	0.11	0.25	0.43	0.13	0.30	0.43	0.14	0.33	0.42
1050	0.09	0.22	0.41	0.11	0.25	0.42	0.12	0.31	0.38
1100	0.08	0.18	0.43	0.09	0.24	0.38	0.10	0.28	0.37

$$\varepsilon_p = 0.018Z^{0.073} \quad [18]$$

The quantitative relationship between these critical conditions of dynamic recrystallization and Zener-Hollomon parameter indicates that the hot deformation behaviour is a thermally activated process.

Flow curve modelling up to peak stress

The flow curve up to peak stress is the region of interest for determination of critical conditions for the initiation of DRX by means of work hardening. Thus, it is becoming increasingly important to be able to calculate the flow stress for specific values of strain, strain rate, and temperature. To model the flow curve up to the peak stress, the flow curve model proposed by Cingara and McQueen can be used (Momeni *et al.*, 2012):

$$\frac{\sigma}{\sigma_p} = [(\frac{\varepsilon}{\varepsilon_p})\exp(1-\frac{\varepsilon}{\varepsilon_p})]^C \quad [19]$$

where σ is stress (MPa), σ_p is the peak stress (MPa), ε is strain, ε_p is the peak strain, and *C* is the material constant.

Taking the natural logarithm of this equation yields the following expression:

$$\ln\frac{\sigma}{\sigma_p} = C[1-\frac{\varepsilon}{\varepsilon_p}+\ln\frac{\varepsilon}{\varepsilon_p}] \quad [20]$$

The experimental data on a logarithmic-scale plot can be used to determine the value of *C*. The plot of $\ln\frac{\sigma}{\sigma_p}$ *vs.* $1-\frac{\varepsilon}{\varepsilon_p}+\ln\frac{\varepsilon}{\varepsilon_p}$ at a strain rate of 5 s^{-1} is shown in Figure 6, and the average value of *C* at all deformation conditions was calculated to be 0.519.

By using the average value of *C*, the predicted flow curves up to the peak strain are shown in Figure 7, which indicate that the models give a better approximation of the flow curve up to the peak.

Processing map

The processing maps not only describes the energy consumption by microstructure evolution during hot deformation, but also visually shows the instability flow regions that should be avoided during the forming process.

The power dissipation through microstructural evolution is represented by a dimensionless efficiency index η as a function of strain rate sensitivity *m*. The efficiency index η can be defined as (Liang *et al.*, 2015; Lou *et al.*, 2014):

$$\eta = \frac{2m}{m+1} \quad [21]$$

where *m* is the strain rate sensitivity exponent, which when the deformation temperature is fixed is a function of the strain rate. The variation of η with deformation temperature and strain rate constitutes a power dissipation map, which represents the power dissipated by the material through microstructural evolution.

The instability criterion parameter ξ(ε̇) is defined as (Liang *et al.*, 2015; Lou *et al.*, 2014)

$$\xi(\dot{\varepsilon}) = \frac{\partial n(\frac{m}{m+1})}{\partial n\dot{\varepsilon}} + m \quad [22]$$

The variation of the instability parameter ξ(ε̇) with ε̇ and *T* at constant strain constitutes an instability map, and flow instability is estimated to occur when ξ(ε̇) becomes negative.

Figure 8 shows the typical processing maps of Nb-Ti microalloyed high-strength steel during hot working at strains of 0.4 and 0.6. The information obtained from the processing map can be used to guide industrial production. First, the temperature and strain rate corresponding to high η represent the optimum working area for the investigated steel, because a high η means that the evolution of microstructure consumes a greater proportion of energy. Secondly, the deformation conditions for

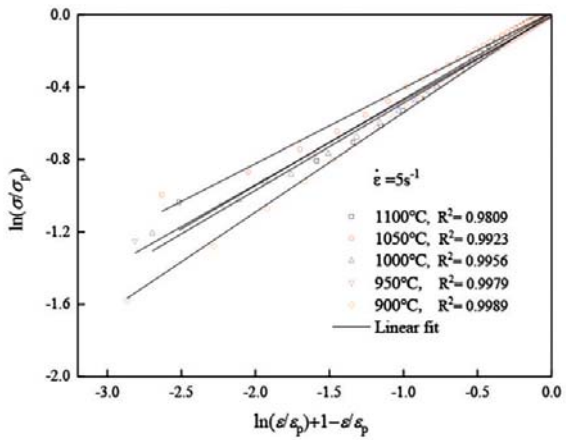

Figure 6—Regression analysis of experimental data at a strain rate of 5 s^{-1} according to the Cingara-McQueen equation

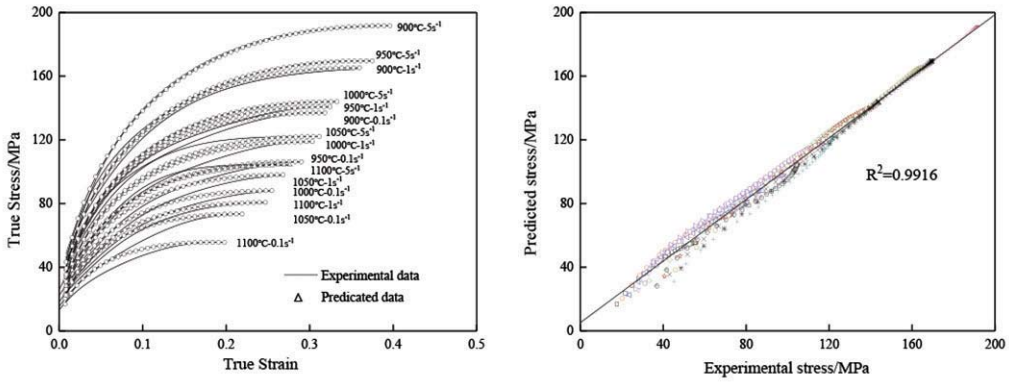

Figure 7—Prediction of flow curves at different deformation conditions

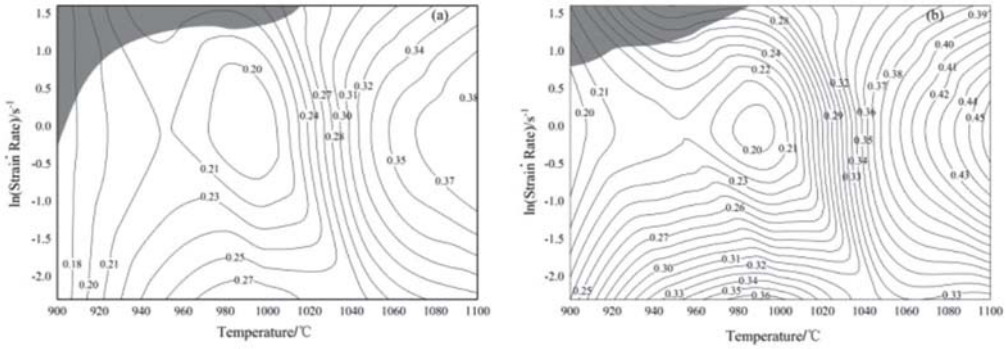

Figure 8—The processing map at strains of (a) 0.4 and (b) 0.6, showing regions of instability

avoiding flow instability can be obtained from the processing map. As shown in Figure 8, the flow instability region appears at deformation temperature between 1010 and 1100°C when the strain rate exceeds 0.78 s^{-1}.

Conclusions

(1) The flow stress is strongly dependent on deformation temperature and strain rate. DRX occurs at a high temperature and low strain rate, which is found to be the main flow softening mechanism in almost all deformation conditions.

(2) The calculated deformation activation energy of the Nb-Ti HSLA steel is about 404 699 J/mol. The constitutive equation is derived as:

$$\dot{\varepsilon} = 1.20\times10^{16} \times [\sinh(0.0087\sigma_p)]^{6.20} \exp(-\frac{404699}{RT}) \quad [23]$$

(3) The characteristics of DRX at different deformation conditions are extracted from the stress-strain curves. Using the work hardening parameter, the value of $\varepsilon_c/\varepsilon_p$ is found to be 0.41. The critical and peak strain can be expressed as $\varepsilon_c = 0.0064Z^{0.077}$, $\varepsilon_p = 0.018Z^{0.073}$. The Cingara-MuQueen equation can model the flow stress accurately up to peak stress for the investigated steel.

(4) Processing map for strains of 0.4 and 0.6 were constructed, and the results show that an instability region exists at a temperature range between 1010 and 1100°C when the strain rate exceeds 0.78 s^{-1}.

References

Banerjee, S., Robi, P.S., and Srinivasan, A. 2012. Deformation processing maps for control of microstructure in Al-Cu-Mg alloys microalloyed with Sn. *Metallurgical and Materials Transactions A*, vol. 43, no.10. pp. 3834–3849.

Cabrera, J.M., Omar, A.A., Prado, J.M., and Jonas, J.J. 1997. Modeling the flow behavior of a medium carbon microalloyed steel under hot working conditions. *Metallurgical and Materials Transactions A*, vol. 28, no. 11. pp. 2233–2244.

Chen, B.H. and Yu, H. 2012. Hot ductility behavior of V-N and V-Nb microalloyed steels. *International Journal of Minerals, Metallurgy and Materials*, vol. 19, no. 6. pp. 525–529.

Chen, X.M., Lin, Y.C., Chen, M.S., Li, H.B., Wen, D.X., Zhang, J.L., and He, M. 2015. Microstructural evolution of a nickel-based superalloy during hot deformation. *Materials and Design*, vol. 77. pp. 41–49.

Churyumov, A.Y., Khomutov, M.G., Solonin, A.N., Pozdniakov, A. V., Churyumova, T.A., and Minyaylo, B.F. 2015. Hot deformation behaviour and fracture of 10CrMoWNb ferritic-martensitic steel. *Materials and Design*, vol. 74, no. 5. pp. 44–54.

Ferdowsi, M.R.G., Nakhaie, D., Benhangi, P.H., and Ebrahimi, G.R. 2014. Modeling the high temperature flow behavior and dynamic recrystallization kinetics of a medium carbon microalloyed steel. *Journal of Materials Engineering and Performance*, vol. 23, no. 3. pp. 1077–1087.

Guo, B.F., Ji, H.P., Liu, X.G., Gao, L., Dong, R.M., Jin, M., and Zhang, Q.H. 2012. Research on flow stress during hot deformation process and processing map for 316LN austenitic stainless steel. *Journal of Materials Engineering and Performance*, vol. 21, no. 7. pp.1455–1461.

Liang, H.Q., Nan, Y., Ning, Y.Q., Li, H., Zhang, J.L., Shi, Z.F., and Guo, H.Z. 2015. Correlation between strain-rate sensitivity and dynamic softening behavior during hot processing. *Journal of Alloys and Compounds*, vol. 632. pp. 478–485.

Lou, Y., Chen, H., Ke, C.X., and Long, M. 2014. Hot tensile deformation characteristics and processing map of extruded AZ80 Mg alloys. *Journal of Materials Engineering and Performance*, vol. 23, no.5. pp. 1904–1914.

Li, L., Li, H.Z, Liang, X.P., Huang, L., and Hong, T. 2015. Flow stress behavior of high-purity Al-Cu-Mg alloy and microstructure evolution. *Journal of Central South University*, vol. 22, no. 3. pp. 815–820.

Mirzadeh, H. and Najafizadeh, A. 2010. Prediction of the critical conditions for initiation of dynamic recrystallization. *Materials and Design*, vol. 31, no. 3. pp. 1174–1179.

Mirzadeh, H., Cabrera, J.M., and Najafizadeh, A. 2012. Modeling and prediction of hot deformation flow curves. *Metallurgical and Materials Transactions A*, vol. 43, no. 1. pp. 108–123.

Momeni, A., Dehghani, K., Heidari, M., and Vaseghi, M. 2012. Modeling the flow curve of AISI 410 martensitic stainless steel. *Journal of Materials Engineering and Performance*, vol. 21, no. 11. pp. 2238–2243.

Momeni, A., Dehghanib, K., and Poletti, M.C. 2013. Law of mixture used to model the flow behavior of a duplex stainless steel at high temperatures. *Materials Chemistry and Physics*, vol. 139. no. 2-3. pp. 747–755.

Opiela, M. 2014. Effect of thermomechanical processing on the microstructure and mechanical properties of Nb-Ti-V microalloyed steel. *Journal of Materials Engineering and Performance*, vol. 23, no. 9. pp. 3379–3388.

Pan, H., Wang, Z.D., Zhou, N., Hui, Y.J., Wu, K.M., and Deng, X.T. 2017. Research on the performance uniformity of 700 MPa grade Ti-microalloying high strength steel. *Steel Rolling*, vol. 34, no. 2. pp.7–13.

Poliak, E.I. and Jonas, J.J. 2003. Initiation of dynamic recrystallization in constant strain rate hot deformation. *ISIJ International*, vol. 43, no. 5. pp. 684–691.

Quan, G.Z., Lv, W.Q., Liang, J.T., Pu, S.A., Luo, G.C., and Liu, Q. 2015. Evaluation of the hot workability corresponding to complex deformation mechanism evolution for Ti–10V–2Fe–3Al alloy in a wide condition range. *Journal of Materials Processing Technology*, vol. 221. pp. 66–79.

Rajamuthamilselvan, M. and Ramanathan, S. 2012. Development of processing map for 7075Al/20% SiCp composite. *Journal of Materials Engineering and Performance*, vol. 21, no. 2 pp. 191–196.

Solhjoo, S. 2010. Determination of critical strain for initiation of dynamic recrystallization. *Materials and Design*, vol. 31, no. 3. pp. 1360–1364.

Shukla, R., Das, S.K., Ravikumar, B., Ghosh, S.K., Kundu, S., and Chatterjee, S. 2012. An ultra-low carbon, thermomechanically controlled processed microalloyed steel: microstructure and mechanical properties. *Metallurgical and Materials Transactions A*, vol. 43, no. 12. pp. 4835–4845.

Wu, L.Z., Li, X.S., Chen, J., Zhang, H.B., and Cui, Z.S. 2010. Dynamic recrystallization behavior and microstructural evolution in SPHC steel. *Journal of Shanghai Jiaotong University (Science)*, vol. 15, no. 3. pp. 301–306.

Wang, M.H., Huang, L., Chen, M.L., and Wang, Y.L. 2015. Processing map and hot working mechanisms of Cu-Ag alloy in hot compression process. *Journal of Central South University*, vol. 22, no. 3. pp. 821–828.

Wu, G.L., Zhou, C.Y., and Liu, X.B. 2017. Static recrystallization behavior of Ti-Nb microalloyed high strength steel. *Journal of the Southern African Institute of Mining and Metallurgy*, vol. 117, no. 5. pp. 451–456.

Yang, Z.Q., Liu, Y., Tian, B.H., and Zhang, Y. 2014. Model of critical strain for dynamic recrystallization in 10%TiC/Cu–Al_2O_3 composite. *Journal of Central South University*, vol. 21, no. 11. pp. 4059–4065.

Zhang, W.F., Sha, W., Yan, W., Wang, W., Shan, Y.J., and Ke, Y. 2014. Constitutive modeling, microstructure evolution, and processing map for a nitride-strengthened heat-resistant steel. *Journal of Materials Engineering and Performance*, vol. 23, no. 8. pp. 3042–3050. ◆